Published for SISSA by Springer

Received: September 23, 2011
Revised: November 8, 2011
Accepted: November 11, 2011
Published: November 24, 2011

Reducing combinatorial uncertainties: a new technique based on M_{T2} variables

Kiwoon Choi,[a] **Diego Guadagnoli**[b] **and Chan Beom Park**[c]

[a] *Department of Physics, KAIST, Daejeon 305-701, Korea*

[b] *Laboratoire de Physique Théorique, Université Paris-Sud, Centre d'Orsay, F-91405 Orsay-Cedex, France*

[c] *Instituto de Física Teórica UAM/CSIC, Nicolás Cabrera 13-15, Universidad Autónoma de Madrid, Cantoblanco, 28049, Madrid, Spain*

E-mail: kchoi@kaist.ac.kr, diego.guadagnoli@th.u-psud.fr, chanbeom.park@csic.es

Abstract: We propose a new method to resolve combinatorial ambiguities in hadron collider events involving two invisible particles in the final state. This method is based on the kinematic variable M_{T2} and on the M_{T2}-assisted-on-shell reconstruction of invisible momenta, that are reformulated as 'test' variables T_i of the correct combination against the incorrect ones. We show how the efficiency of the single T_i in providing the correct answer can be systematically improved by combining the different T_i and/or by introducing cuts on suitable, combination-insensitive kinematic variables. We illustrate our whole approach in the specific example of top anti-top production, followed by a leptonic decay of the W on both sides. However, by construction, our method is also directly applicable to many topologies of interest for new physics, in particular events producing a pair of undetected particles, that are potential dark-matter candidates. We finally emphasize that our method is apt to several generalizations, that we outline in the last sections of the paper.

Keywords: Heavy Quark Physics, Hadronic Colliders

ArXiv ePrint: 1109.2201

doi:10.1007/JHEP11(2011)117

Contents

1 Introduction

Many models providing WIMP dark-matter candidates predict events at the Large Hadron Collider (LHC), characterized by a pair of invisible particles in the final state. This very same topology is also available in the Standard Model (SM), e.g. in dileptonic decays of a top-quark pair: $t\bar{t} \to b\ell^+\nu\bar{b}\ell^-\bar{\nu}$. Several kinematic methods have been proposed to determine the particle masses in such missing energy events [1]. On the other hand, to access information beyond the mass, e.g. the spin and/or chirality of parent particles, it is very often highly desirable, sometimes necessary, to reconstruct the parent particles' full momenta event by event. Such reconstruction generically suffers from the combinatorial ambiguity of correctly assigning visible particles to the given event topology. For instance, there are two possibilities to pair the two b-jets and the two charged leptons in the dileptonic decay of a top quark pair, and three possibilities to group the jets into two dijets in the gluino pair decay $\tilde{g}\tilde{g} \to jj\tilde{\chi}_1^0 jj\tilde{\chi}_1^0$ in supersymmetric models, $\tilde{\chi}_1^0$ denoting the LSP neutralino. Not to mention that the possible combinations proliferate when the event involves multi-step cascade decays and one wishes to identify the order of visible particles in each decay chain, besides the assignment to the correct decay chain. For instance, in the event $\tilde{\chi}_2^0\tilde{\chi}_2^0 \to \tilde{\ell}^\pm\ell^\mp\tilde{\ell}^\pm\ell^\mp \to \ell^+\ell^-\tilde{\chi}_1^0\ell^-\ell^+\tilde{\chi}_1^0$, one has in total $2\times 2\times 2 = 8$ possibilities to assign the charged leptons to the event topology (assuming they have all the same flavor), and even more to correctly assign jets in the cascade decay $\tilde{g}\tilde{g} \to j\tilde{q}j\tilde{q} \to jj\tilde{\chi}_1^0jj\tilde{\chi}_1^0$ $(3\times 2\times 2 = 12)$.

Quite generally, it is clear that minimizing combinatorial uncertainties is one of the first steps toward an accurate reconstruction of the full parent particles' momenta in missing energy events.[1] Actually, this problem is already relevant within the SM, with no need to invoke new-physics events. A well-known example is that of dileptonic $t\bar{t}$ events in the SM, where the reconstruction of the t and $\bar{t}$ momenta is required in order to study spin correlations in $t\bar{t}$ [3–6], which in turn allow to probe the quantum structure of the decay much more thoroughly than the information from the cross section alone does. Broadly speaking, strategies aimed at fully reconstructing the *momenta* of parent particles in missing-energy events are of obvious relevance when it comes to making the most out of the LHC data.

In this paper, we aim to develop a model-independent way of reducing combinatorial uncertainties for missing energy events at the LHC. We propose a new method based on the combined use of the kinematic variable M_{T2} [7, 8] and of the M_{T2}-assisted-on-shell (MAOS) reconstruction of missing momenta [9]. All these kinematic variables are reformulated as 'test' variables T_i (testing the correct pairing of final-state visible particles against the incorrect ones) and the information from the various T_i is then used combinedly, in order to improve over the performance of each T_i separately.

We apply this strategy to the dileptonic $t\bar{t}$ decay, that, as mentioned, represents a prototype example of pair production of a parent particle of interest decaying into partly-invisible daughters. Besides its intrinsic interest, the $t\bar{t}$ decay offers a popular event topology in SM extensions with a dark-matter candidate, rendered stable by a conserved Z_2-like symmetry. Applying our method to dileptonic $t\bar{t}$, we find an efficiency of determining the correct partition in the ballpark of 90%, and that this efficiency can be systematically increased by introducing cuts on certain partition-insensitive kinematic variables, at the price of an actually moderate loss in event statistics.

The organization of our paper is best summarized in the table of content. In section 2 we start with an example of the problem at hand, and then introduce our test variables T_i in terms of M_{T2} and of the MAOS algorithm, applied to the full $t\bar{t}$ decay or to its WW subsystem. We here examine the efficiency of each variable T_i in the context of a parton-level analysis. In section 3, we address the issue of improving over the efficiency of each single T_i, by devising a combined test, and introducing the above mentioned cut variables. In section 4, we discuss some generalizations of our method, in particular its application to generic missing energy events producing a pair of dark matter particles in the final state. Finally, in section 5 we conclude, providing an outlook of future work.

[1] For example, see the method recently proposed in ref. [2].

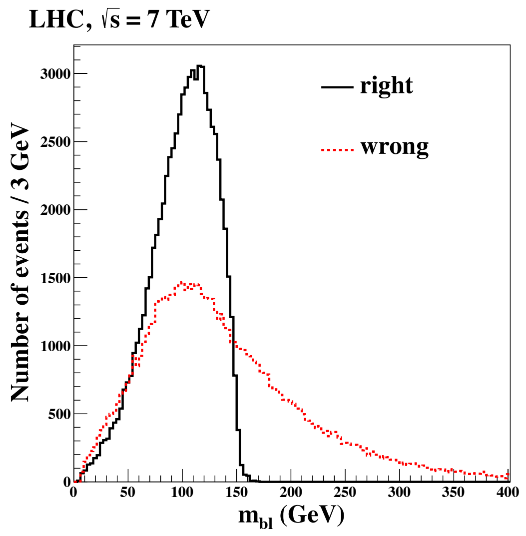

Figure 1. The $m_{b\ell}$ distribution for the $t\bar{t}$ event topology (2.1) with right (solid black) and wrong (red dashed) partitions of the b quarks and charged leptons. The event generation details for this and the rest of our plots are described in section 2.2.

2 Test variables to choose among partitions of the visible final states

2.1 An example

We will state our problem of interest in the example of $t\bar{t}$ production followed by fully leptonic W decays. The decay chain is namely

$$t\bar{t} \to bW^+ \, \bar{b}W^- \to b\ell^+\nu \, \bar{b}\ell^-\bar{\nu} \; . \tag{2.1}$$

At the level of reconstructed objects, this process is triggered on by, e.g., requiring at least two jets (two of which possibly b-tagged), two leptons and missing energy in the final state. Clearly, the triggered-on objects can be partitioned in two different ways, namely

$$\begin{aligned} \text{right partition} &\equiv \{\ell_1 b_1\}\&\{\ell_2 b_2\} \, , \\ \text{wrong partition} &\equiv \{\ell_1 b_2\}\&\{\ell_2 b_1\} \, , \end{aligned}$$

where the index labels the decay chain. In the rest of the text we will refer to the different ways of grouping visible final states into two sets as partitions.

Our aim is to construct test variables able to distinguish the right from the wrong final-state partitions. To this end, one may exploit suitable event variables, that namely display certain predictable features as a function of the event kinematics — like edges, thresholds or peaks. The main observation to take advantage of is that these features are present, and calculable from the measured final states, *provided* the partition of the visible particles is the right one, whereas they are partly or completely destroyed if the final-state partition is incorrect.

The arguably simplest and best-known example to illustrate such ideas is the invariant mass of the visible particles, m_{V_i}, belonging to a given decay chain i. In the case of the

JHEP11(2011)117

event topology (2.1), the visible particles of each decay chain are a b-quark and a charged lepton. The corresponding invariant mass distribution enjoys an upper endpoint given by the formula

$$\begin{aligned}(m_{b\ell}^{\max})^2 &= m_b^2 + \frac{1}{2}\left(m_t^2 - m_W^2 - m_b^2\right) + \frac{1}{2}\sqrt{\left(m_t^2 - m_W^2 - m_b^2\right)^2 - 4m_W^2 m_b^2} \\ &\simeq 153.2\,\text{GeV}\ .\end{aligned} \tag{2.2}$$

This endpoint feature is clearly displayed by the black solid histogram in figure 1, representing the $m_{b\ell}$ distribution when correctly partitioning the final states. The same feature does not need to hold in case $m_{b\ell}$ is calculated with the incorrect final-state partition: the corresponding histogram is also shown as a red dashed curve. Indicating the two possible partitions as P_1 and P_2, one can then construct the *difference* between the $m_{b\ell}$ values calculated with either partition, namely

$$\Delta T(P_2,\, P_1) \equiv T(P_2) - T(P_1)\,, \tag{2.3}$$

where

$$T(P_i) \equiv m_{b\ell}(P_i) \tag{2.4}$$

is the test variable for a given partition P_i. From our previous considerations, one can expect that, if P_1 corresponds to the right partition, P_R, and P_2 to the wrong one, P_W, then $\Delta T(P_W,\, P_R)$ is expected to be *larger than zero*, at least for a subset of the possible kinematic configurations of the visible final states.

We therefore introduce the following criterion for using $\Delta T(P_2,\, P_1)$ as a variable testing the correct final-state partition in the case of dileptonic $t\bar{t}$ decay:

Given a final state of $2b$-jets $+2\ell$, they can be partitioned in two possible ways, to be called P_1 and P_2. If $\Delta T(P_2,\, P_1)$, defined as eq. (2.3), is found to be > 0 (< 0), then P_1 (P_2) may be identified as the correct partition, with a calculable probability p of misidentification.

In the sections to follow we will introduce several such *test* variables $T(P)$, and for each of them estimate the efficiency $1 - p$. We will also see that this efficiency can be systematically improved in two directions:

(i) by introducing further kinematic cuts on the event sample, at the price of a reduced statistics;

(ii) by combining the information from several $T(P)$ in a global test variable, for example, a likelihood test with the $\Delta T(P_2,\, P_1)$ distributions interpreted as probability distributions.

Both of the above points will be addressed in the sections starting from section 3. All the numerical results of our paper rely on event simulations, whose details are introduced in the next section 2.2. In the rest of section 2 we will introduce all the test variables and discuss variations around their definitions as well as their efficiencies.

2.2 Event generation and selection

We generated 100,000 parton-level events of top quark pair production followed by dileptonic final states using `MadGraph 5`, with proton-proton collisions at $\sqrt{s} = 7\,\text{TeV}$ [10]. We here do not assume any contribution from physics beyond the SM. The SM predicts $\sigma_{t\bar{t}} \sim 162$ pb at next-to-next-to-leading-order [11].[2] Hence the generated events correspond to $\sim 13\,\text{fb}^{-1}$. The dilepton mode gives rise to final states with two b-tagged jets, two leptons, missing transverse energy. We consider the leptonic decays of the W bosons to an electron or muon.[3]

We apply event selection cuts on the simulated event sample following the $0.7\,\text{fb}^{-1}$ ATLAS dileptonic top analysis [13]. We namely require

- exactly two oppositely-charged leptons (ee, $\mu\mu$, $e\mu$) with $p_T > 25\,\text{GeV}$ and $|\eta| < 2.5$,
- at least two jets with $p_T > 25\,\text{GeV}$ and $|\eta| < 2.5$,
- dilepton invariant mass, $m_{\ell\ell} > 15\,\text{GeV}$,
- that events in the same-flavor lepton channels must satisfy the missing transverse energy condition $\not{E}_T > 60\,\text{GeV}$ and $|m_{\ell\ell} - m_Z| > 10\,\text{GeV}$,
- that events in the different-flavor channel satisfy $H_T > 130\,\text{GeV}$. The event variable H_T is defined as the scalar sum of the transverse momenta of the two leptons and all selected jets. In analogy with [13] we instead do not require $\not{E}_T$ or $m_{\ell\ell}$ cuts in this channel.

We found that about 37% of the total simulated events pass these basic selection cuts. The motivation for including the mentioned cuts is to have an event sample that resembles as much as possible the actual experimental event samples in dileptonic $t\bar{t}$ production. As such, it will be our reference event sample throughout our analysis. We leave aside for the moment the important issues of: inclusion of hadronization, QCD radiation, and modeling of detector effects, that we will address in a forthcoming, more in-depth study [14].

2.3 Test variables: definition and discussion

2.3.1 Invariant mass of visible final states: T_1 variable

Our first test variable is constructed from $m_{b\ell}$, mentioned in the example of section 2.1. In particular, it could be defined directly as in eq. (2.4). However, for each event one obtains two $m_{b\ell}$ values, $m_{b\ell}^{(i)}$ ($i = 1, 2$), corresponding to the two decay chains. Combining the two $m_{b\ell}^{(i)}$ values in different ways gives rises to alternative definitions of the test variable, not all of which yield the same efficiency. We found the combination $\max[m_{b\ell}^{(1)}, m_{b\ell}^{(2)}]$ to perform best:

$$\max\left[m_{b\ell}^{(1)}, m_{b\ell}^{(2)}\right](P_W) > \max\left[m_{b\ell}^{(1)}, m_{b\ell}^{(2)}\right](P_R) : 80.2\% \,. \tag{2.5}$$

[2]The cross section was calculated with $m_t = 173\,\text{GeV}$ and CTEQ6.6 parton distributions [12].

[3]There are small contributions from the leptonic decays of the tau, for example, $\tau^- \to \mu^- \bar{\nu}_\mu \nu_\tau$, but here we neglect them for the sake of discussion.

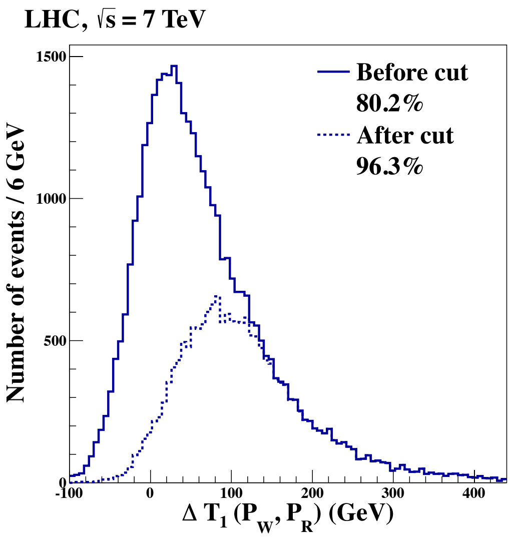

Figure 2. Distribution for the variable $\Delta T_1(P_W, P_R)$ (see defs. in eqs. (2.6) and (2.3)) with P_W and P_R denoting the wrong and the right partition respectively. The legend in the plot indicates the percentage of correctly partitioned events, before and after inclusion of the cut $M_T^{t\bar{t}}(0) > 400\,\text{GeV}$, to be described in section 3.2.

We correspondingly define our first test variable as follows:

$$T_1(P_i) \equiv \max\left[m_{b\ell}^{(1)},\, m_{b\ell}^{(2)}\right](P_i)\,, \tag{2.6}$$

for a given partition P_i. The $\Delta T_1(P_W, P_R)$ distribution is shown in figure 2.

The efficiency figure in eq. (2.5), as well as in the solid histogram in figure 2, refers to the events that pass the basic selection cuts described in section 2.2, and actually includes one further consideration: if one of the partitions results in $m_{b\ell} > m_{b\ell}^{\max}$, then the right partition can be clearly selected because $m_{b\ell}(P_R) \le m_{b\ell}^{\max}$.

2.3.2 M_{T2} of the whole decay chain: T_2 variable

Another event variable that may be used to construct a test variable of correct partitioning is M_{T2}, the so-called "stransverse mass", which is especially suited to topologies with pair-produced particles, each decaying into partly invisible final states [7, 8]. The general event topology that M_{T2} is suited for is the following:

$$Y\bar{Y} \;\to\; V_1(p_1)\chi(k_1) + V_2(p_2)\bar{\chi}(k_2)\,, \tag{2.7}$$

where each of the V_i denotes a (set of) visible state(s), whose total four-momentum is, in principle, entirely reconstructible, and χ, $\bar{\chi}$ denote invisible particles with identical mass. The decay mode (2.1) is an example of this very event topology: V_i should be identified with a $b\,\ell$ pair (for each decay chain) and $\chi, \bar{\chi}$ with the neutrinos.

For the event topology (2.7), the M_{T2} variable is defined as

$$M_{T2}(\tilde{m}_\chi) \equiv \min_{\tilde{\mathbf{k}}_{1T}+\tilde{\mathbf{k}}_{2T}=\not{\mathbf{p}}_T}\left[\max\left\{M_T^{(1)}\left(\mathbf{p}_{1T},\, \tilde{\mathbf{k}}_{1T},\, p_1^2,\, \tilde{m}_\chi\right),\, M_T^{(2)}\left(\mathbf{p}_{2T},\, \tilde{\mathbf{k}}_{2T},\, p_2^2,\, \tilde{m}_\chi\right)\right\}\right], \tag{2.8}$$

where $M_T^{(i)}$ is the transverse mass [15, 16] of the decay chain $i\,(=1$ or $2)$, namely

$$\left(M_T^{(i)}\right)^2 = p_i^2 + \tilde{m}_\chi^2 + 2\left(\sqrt{|\mathbf{p}_{\mathbf{i}T}|^2 + p_i^2}\sqrt{|\tilde{\mathbf{k}}_{\mathbf{i}T}|^2 + \tilde{m}_\chi^2} - \mathbf{p}_{\mathbf{i}T}\cdot\tilde{\mathbf{k}}_{\mathbf{i}T}\right)\,. \tag{2.9}$$

A few comments may help get an intuitive picture of the above definitions. First, it should be kept in mind that what is measured in the event topology of (2.7) are the visible particles' momenta, p_i, and the total momentum imbalance in the transverse direction, $\not{\mathbf{p}}_T$. The definition in eq. (2.8) correspondingly marginalizes over the transverse momenta $\mathbf{k}_{\mathbf{1},\mathbf{2}T}$ of χ, $\bar{\chi}$, that are not separately measured, by taking the minimum over all the *trial* momentum configurations (denoted with a tilde), whose sum equals the measured $\not{\mathbf{p}}_T$.

Second, the invisible mass m_χ is, likewise, unmeasured, hence M_{T2} is a function of a trial value for this mass, $\tilde{m}_\chi$. In the case of the decay (2.1) m_χ is of course known: $m_\chi = m_\nu \approx 0$. However, the topology in eq. (2.7) applies also to several new-physics scenarios, and in this case the physical mass m_χ of the pair-produced χ is in general unknown. An interesting feature of M_{T2} is the kink structure of $M_{T2}^{\max}(\tilde{m}_\chi)$ at $\tilde{m}_\chi = m_\chi$, provided the p_i^2 value spans a certain range in each decay chain [17, 18]. An alternative possibility for the kink structure of $M_{T2}^{\max}(\tilde{m}_\chi)$ to appear is to have the $Y\bar{Y}$ system boosted by a sizable amount of upstream transverse momentum [19, 20]. The M_{T2}-kink method makes it possible to measure m_χ and m_Y *simultaneously*, and even if the decay chain is not long enough to constrain all the unknowns in the event.

The property of M_{T2} most relevant to our discussion is that, when the input trial mass $\tilde{m}_\chi$ equals the true mass value m_χ, the upper endpoint of the M_{T2} distribution corresponds to the parent particle mass m_Y. We want to use this property to distinguish the correct against the incorrect partition of the final-state visible particles. We note explicitly that, in dileptonic $t\bar{t}$, one can construct two kinds of M_{T2}: $M_{T2}^{t\bar{t}}$ for the full $t\bar{t}$ system and M_{T2}^{WW} for the WW subsystem [21–24], the visible particles being respectively $b\ell^+\bar{b}\ell^-$ and $\ell^+\ell^-$. Since only one partition is possible in M_{T2}^{WW}, this variable cannot be used directly as a test variable. It can however be used to construct other test variables, to be introduced in the next section. In the rest of the present discussion we will therefore specialize to $M_{T2}^{t\bar{t}}$.

As already mentioned, the $M_{T2}^{t\bar{t}}$ distribution is bounded from above by the top quark mass m_t if the partition is the right one, whereas it is not if the partition is the wrong one. This fact is shown in the left panel of figure 3. One can therefore define the variable

$$T_2(P_i) \equiv M_{T2}^{t\bar{t}}(P_i)\,, \tag{2.10}$$

where we recall that P_i $(i = 1, 2)$ denotes the two possible partitions of the $2b + 2\ell$ visible final states.

In the right panel of figure 3, we show the distribution of $\Delta T_2(P_W, P_R)$ with the right (P_R) and wrong (P_W) partitions. The figure shows that the relation $\Delta T_2(P_W, P_R) > 0$ holds for about 80% of the events that passed just the basic selection cuts described in section 2.2, and that this percentage reaches as much as 97% after the $M_T^{t\bar{t}}(0)$ cut to be described in section 3.2.

To conclude this section, we mention that the M_{T2} method of finding the right partition has been proven to be useful for mass measurements and/or event reconstruction in refs. [20, 25–35].

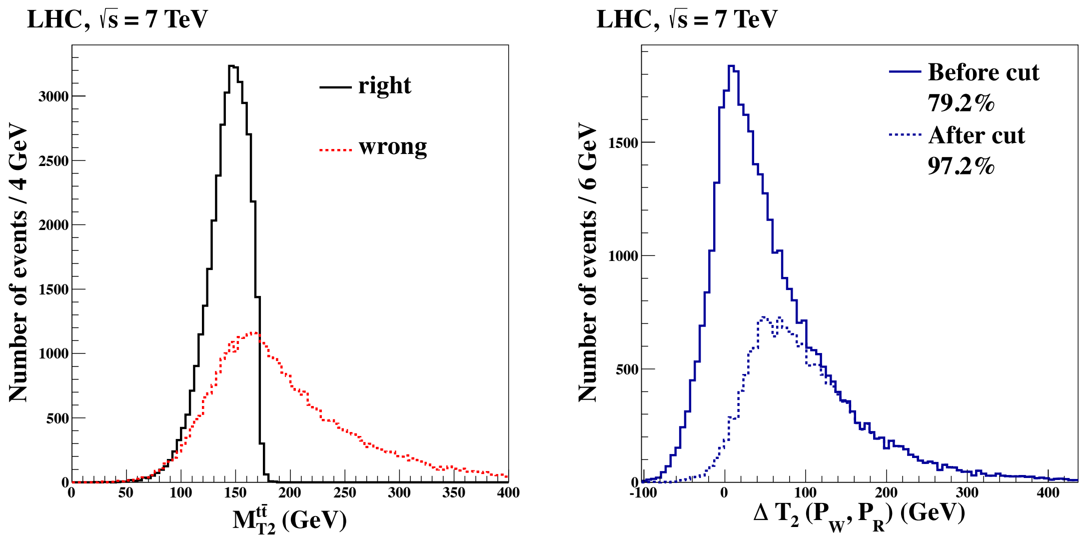

Figure 3. The distributions of $T_2 \equiv M_{T2}^{t\bar{t}}$ (left panel) and $\Delta T_2(P_W, P_R)$ (right panel), with P_W and P_R the wrong and right partitions respectively. The legend in the second panel indicates the percentage of correctly partitioned events, before and after inclusion of the cut $M_T^{t\bar{t}}(0) > 400\,\text{GeV}$, to be described in section 3.2.

2.3.3 MAOS-reconstructed m_t and m_W mass: $T_{3,4}$ variables

A further set of variables to test the correct partition can be constructed from the observation that the sum of final-state momenta in either decay chain must reconstruct, up to width effects, the parent-particle's invariant mass. The main obstacle to this, in the case of the event topology (2.7), is the fact that the invisible momenta of the two decay chains, k_1 and k_2, are not measured separately, but only their sum is, and only in the transverse plane.

Systematic techniques exist however, enabling to obtain a *best guess* of the invisible momenta k_1 and k_2.[4] Among these techniques is the so-called M_{T2}-assisted on-shell (MAOS) reconstruction of invisible momenta [9]. The only assumption of the MAOS method is that the event topology should be of the kind of eq. (2.7). Then the transverse components of the invisible momenta, $\mathbf{k_1}_T$, $\mathbf{k_2}_T$, can be estimated event by event to be the location of the minimum of the M_{T2} variable constructed for the event. Recall in fact that, from eq. (2.8), M_{T2} is obtained from a minimization over all possible $\tilde{\mathbf{k}}_{\mathbf{1,2}T}$ configurations subject to the constraint $\tilde{\mathbf{k}}_{\mathbf{1}T} + \tilde{\mathbf{k}}_{\mathbf{2}T} = \not{\mathbf{p}}_T$.

Once $\mathbf{k_1}_T$ and $\mathbf{k_2}_T$ are estimated by M_{T2}, the longitudinal components of the invisible momenta may be determined from the on-shell relations

$$(p_i + k_i^{\text{maos}})^2 = m_Y^2\,, \quad (k_i^{\text{maos}})^2 = m_\chi^2 \tag{2.11}$$

where, as usual, i labels the decay chain, m_Y the parent particle mass, and m_χ the invisible particle mass. eqs. (2.11) amount to a quadratic equation in the longitudinal components

[4] For the dileptonic $t\bar{t}$ decay, one of the presently most popular techniques is the neutrino weighting method, which has been used for the top quark mass measurement [36, 37] and for studying spin correlations in $t\bar{t}$ production [38].

of k_i, hence one has in general two solutions for each decay chain, $\tilde{k}^{\pm}_{\mathbf{i}L}$. Modulo this two-fold ambiguity, and assuming m_χ to be known (in our case it is $m_\nu \approx 0$), the MAOS reconstruction thus leads to a estimate of the *full* invisible momenta k_i. Specifically, $k_i^{\rm maos}$ has a roughly Gaussian distribution around $k_i^{\rm true}$ and a moderate spread, that can be systematically improved by requiring event cuts [9].

In our case, the whole argument in the previous paragraph can be applied to the full $t\bar{t}$ decay, or to the WW subsystem, because both share the same, mentioned topology (2.7). In particular, from the MAOS momenta of the WW system, $k_{1,2}^{\text{maos-}WW}$, one can construct the invariant mass of the top quark as

$$\left(m_{t,i}^{\rm maos}\right)^2 \equiv \left(p_{b,i} + p_{\ell,i} + k_i^{\text{maos-}WW}\right)^2 , \tag{2.12}$$

whereas from the MAOS momenta of the $t\bar{t}$ system, $k_i^{\text{maos-}t\bar{t}}$, one can construct the W boson invariant mass as

$$\left(m_{W,i}^{\rm maos}\right)^2 \equiv \left(p_{\ell,i} + k_i^{\text{maos-}t\bar{t}}\right)^2 . \tag{2.13}$$

It is clear that, if the right partition is selected and in the limit where the MAOS momenta equal the true momenta in each decay chain, eqs. (2.12) and (2.13) should equal respectively the true m_t and m_W values, up to finite decay widths. In practice, the MAOS momenta differ in general from the true momenta. However, the MAOS invariant mass distribution exhibits a peak structure around the true parent particle mass. Hence — to the extent that the spread around the peak value is not too large — the above eqs. (2.12) and (2.13) are still useful for our purpose, which is, we recall, not to measure the t or W mass, but to single out the correct final-state partition. We show in figure 4 the $m_t^{\rm maos}$ (left panel) and the $m_W^{\rm maos}$ (right panel) distributions calculated using the right partition (black solid histogram) and the wrong partition (red dashed histogram).

The argument below eqs. (2.12)–(2.13) may be used to construct a test variable of correct partition by noting that

$$|m_{t,i}^{\rm maos} - m_t|(P_W) > |m_{t,i}^{\rm maos} - m_t|(P_R) , \tag{2.14}$$

and a similar inequality holds also for $m_W^{\rm maos}$. In reality, the notation in relation (2.14) is incomplete, because of the mentioned discrete ambiguity in the determination of the longitudinal components of the invisible momenta. This is a common problem for methods attempting to reconstruct invisible momenta, and based on polynomial on-shell equations of degree higher than one. One cannot distinguish the solutions among themselves, even though only one solution corresponds to the true one and the others are redundant.

We construct our test variable treating these solutions in a symmetric way. We first define a quantity

$$\Delta_t m_t^{\rm maos}(\alpha) \equiv m_t^{\rm maos}(p_b,\, p_l,\, k^\alpha) - m_t \quad (\alpha = +,\, -) , \tag{2.15}$$

where we omitted the chain label, and α denotes the two MAOS solutions for the invisible momentum $k^{\rm maos}$ in that decay chain. Thence we found that

$$\sum_{i=1,2;\,\alpha=+,-} |\Delta_t m_{t,i}^{\rm maos}(\alpha)|(P_W) > \sum_{i=1,2;\,\alpha=+,-} |\Delta_t m_{t,i}^{\rm maos}(\alpha)|(P_R) : 84.2\% , \tag{2.16}$$

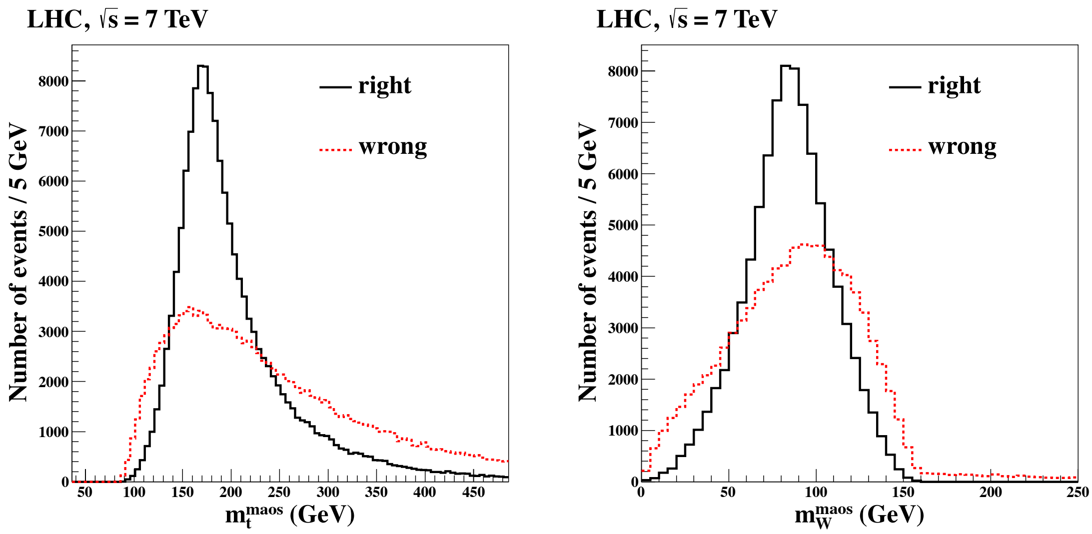

Figure 4. The m_t^{maos} (left panel) and m_W^{maos} (right panel) distributions for the right and for the wrong final-state partition. The distributions include only events with real MAOS solutions for all partitions (see text for details).

namely that the sum over chains and over $k^{\pm}$ solutions of the quantity defined in (2.15) is smaller when calculated on the right partition than on the wrong partition in as much as 84% of the events.[5] Consistently with the discussion in section 2.1, we then define our test variable T_3 as follows:

$$T_3(P_k) \equiv \sum_{i=1,2;\,\alpha=+,-} |\Delta_t m_{t,i}^{\text{maos}}(\alpha)|(P_k)\ . \tag{2.17}$$

The whole line of reasoning below eq. (2.14) can be applied to the WW subsystem as well. Similarly as m_t^{maos} in (2.15) one constructs the difference between m_W^{maos} and m_W and symmetrizes between decay chains and $k^{\pm}$ solutions. We obtained

$$\sum_{i=1,2;\,\alpha=+,-} |\Delta_W m_{W,i}^{\text{maos}}(\alpha)|(P_W) > \sum_{i=1,2;\,\alpha=+,-} |\Delta_W m_{W,i}^{\text{maos}}(\alpha)|(P_R) : 86.8\%\,, \tag{2.18}$$

and we define our test variable T_4 as

$$T_4(P_k) \equiv \sum_{i=1,2;\,\alpha=+,-} |\Delta_W m_{W,i}^{\text{maos}}(\alpha)|(P_k)\ . \tag{2.19}$$

An important difference between the m_t^{maos}-based method and the m_W^{maos}-based one should be emphasized. Within the m_t^{maos} method, the choice of final-state partition enters only when constructing the top invariant mass (see eq. (2.12)), whereas only one partition is possible in the estimate of $k_i^{\text{maos-}WW}$. Conversely, within the m_W^{maos} method, the choice

[5]We mention that we have tried a number of alternative combinations besides $\sum_{i=1,2;\,\alpha=+,-}|\cdot|$. In particular $\prod_{\alpha,\beta=+,-}|\cdot|$, $\sum_{i=1,2;\,\alpha=+,-}|\cdot|^2$, $\min_{\alpha,\beta=+,-}|\cdot|$ and $\max_{\alpha,\beta=+,-}|\cdot|$. The combination proposed in eq. (2.16) is the one found to have the best efficiency.

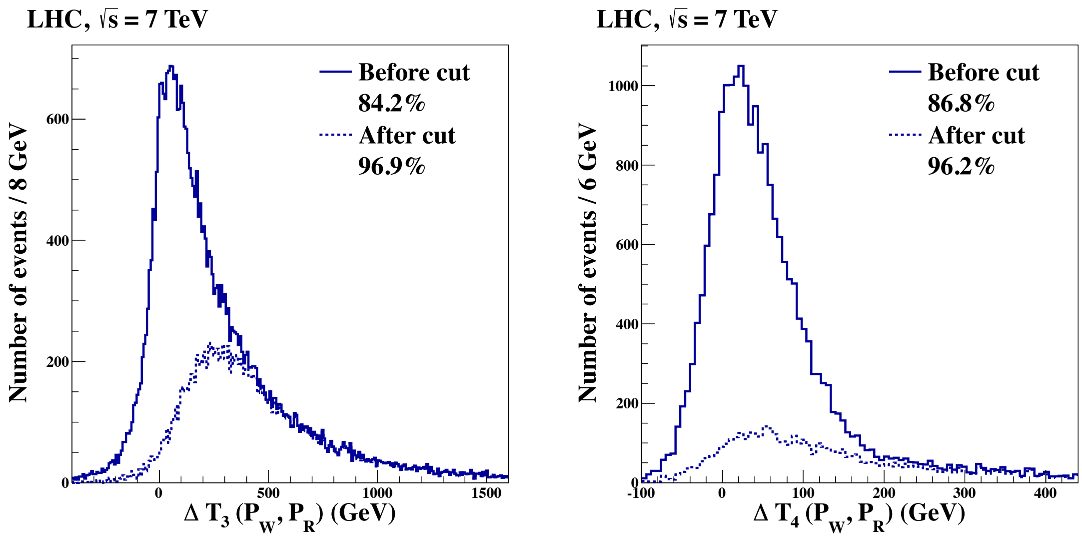

Figure 5. The distributions of $\Delta T_3(P_W, P_R)$ (left panel) and $\Delta T_4(P_W, P_R)$ (right panel), with P_W and P_R denoting the wrong and the right partition. The legend indicates the percentage of correctly partitioned events, before and after inclusion of the cut $M_T^{t\bar{t}}(0) > 400\,\text{GeV}$, to be described in section 3.2. The efficiency figures in the right panel take into account the complex-MAOS-solution criterion, whereas histograms report only the events free of complex solutions. See text for full details.

of final-state partition does come into play in the calculation of $k_i^{\text{maos-}t\bar{t}}$ (see eq. (2.13)), namely when calculating M_{T2} of the $t\bar{t}$ system. The important point is that *wrong* partitions sometimes result in *complex* solutions for (the longitudinal components of) $k_i^{\text{maos-}t\bar{t}}$ much more often than *right* partitions do,[6] and this can be used as a further criterion for identifying the right partition. From our simulation, we found that:

(a) events with at least one complex solution (in any of the partitions) occur 38.5% of the time;

(b) most importantly, events where a complex solution appears only in the wrong partition occur 37.9% of the time — very close to the percentage in point (a).[7]

From the above points, it is clear that the m_W^{maos} method can be augmented by the following requirement:

if the MAOS calculation returns at least a complex solution, but only for one of the partitions, then this partition should be regarded as the wrong one.

[6]Right partitions can also yield complex solutions, but only because of occasional failure of the numerical minimization in the M_{T2} calculation, that we find to be the case only for a very small subset of all events (about 0.6%). We used a modified version of the `Mt2::Basic_Mt2_332_Calculator` algorithm of the Oxbridge MT2 / Stransverse Mass Library [39].

[7]Besides, we found: (i) events where a complex solution appears in both the right and the wrong partition (0.4% of the total events). Of course for this kind of events the information from m_W^{maos} is unusable; (ii) events where a complex solution appears only in the right partition (0.2% of the total events). Events (i) and (ii) explain the difference between the percentages in points (a) and (b).

In the following we will refer to this statement as the complex-MAOS-solution criterion. This requirement has a probability of mistakenly discarding a correctly paired event as small as 5 per mil, as can easily be deduced from the above items. Note that this criterion is already taken into account in the 86.8% efficiency figure reported in eq. (2.18) and should be regarded as part and parcel of the ΔT_4 method.

The whole discussion between eq. (2.16) and the previous paragraph is illustrated in the plots of figure 5, that report the distributions for $\Delta T_3(P_W, P_R)$ and $\Delta T_4(P_W, P_R)$ (we recall the reader that ΔT is defined in eq. (2.3)). In particular, the efficiency figures in eqs. (2.16) and (2.18) correspond to the solid-line histograms, namely those before the $M_T^{t\bar{t}}(0)$ cut to be introduced in section 3.2 (see figure legend).

A careful reader may have noted that, in the ΔT_4 panel, the percentage of events in the positive semiaxis looks, and in fact is, smaller that the corresponding efficiency (percentage of correctly partitioned events) indicated in the legend. This is especially true for the histogram after the $M_T^{t\bar{t}}(0)$ cut. The reason is the fact that the T_4-method efficiency is calculated as the sum of the $\Delta T_4 > 0$ criterion *and*, when applicable, of the complex-MAOS-solution criterion, that by itself belongs to the T_4-method, as already mentioned. Schematically, the total T_4-method efficiency, ϵ_{T_4}, splits up as follows:

$$\epsilon_{T_4} \;=\; C \cdot \epsilon_C + R \cdot \epsilon_R \,, \tag{2.20}$$

where C is the percentage of events with complex solutions, R is the percentage of events free of complex solutions ($C + R =$100%), ϵ_C denotes the efficiency of the complex-MAOS-solutions method and ϵ_R the efficiency of the $\Delta T_4 > 0$ method. For the events passing the $M_T^{t\bar{t}}(0)$ cut, we found $R = 31\%$ and $\epsilon_R \simeq 90\%$. The R subset is the only one displayed in the dashed histogram on the right panel of figure 5, and the efficiency ϵ_R is the percentage of this histogram lying in the positive semiaxis. More importantly for the overall method efficiency ϵ_{T_4} in eq. (2.20) is to note that $C = 1 - R = 69\%$ and that $\epsilon_C \simeq 99\%$, to be compared with $C = 38.5\%$ (and ϵ_C basically the same) before the cut. These figures demonstrate that, after the cut, wrongly partitioned events tend to display complex MAOS solutions way more often than before the cut. This behavior is actually expected: if the T_4 variable, constructed with wrongly partitioned kinematics, may produce complex solutions, they will tend to proliferate if the kinematics gets more boosted, as is the case after the cut. The bottom line is that, from the point of view of the overall T_4-method efficiency, an increase in the number of events with complex solutions C is an advantage, because the complex-MAOS-solution criterion has by itself an efficiency ϵ_C of nearly 100% of picking up the correct partition.

To conclude this section, we note explicitly that the previous discussion refers to events at parton level, as assumed throughout this paper. Of course, effects such as momentum smearing may well destabilize the above conclusions. However, it seems reasonable to believe that the main effect of smearing will not be to have complex solutions migrate from the wrong to the right partition, but rather to increase the number of events where *both* the right and wrong partitions consist of only complex solutions. Such events represented only 0.6% of our total events (see point (b) above), and we simply did not use the T_4 variable for such events. It is possible that this fraction of events increases, maybe even substantially, when including mismeasurement effects. Rather than simply disposing of

JHEP11(2011)117

the T_4 variable for these events, one may instead consider introducing some more general complex-solution criterion than the one advocated in this section. One such criterion may be to choose as the true partition the one whose MAOS solution has, for instance, the largest real part. It is worth mentioning that the issue of complex solutions in event reconstruction has been recently discussed in detail in ref. [40], and the argument in the present paragraph is inspired by the main messages in that paper. We leave the question of the utility and efficiency of our thus-reformulated complex-MAOS-solution criterion to forthcoming work [14] where smearing effects will be taken into account.

3 Improving the method efficiency

3.1 Correlations and combinations of the test variables

In the previous section we have shown that each of the introduced test variables T_i is able to find the correct final-state partition in $\gtrsim 80\%$ of the total events that pass the basic selection cuts. Already at the end of section 2.1 we have emphasized that the overall method efficiency may be systematically improved by combining the T_i and/or by introducing appropriate kinematic cuts. We will now address these two possibilities in turn.

First of all, the possibility that combining the T_i does indeed allow to increase the overall method efficiency relies on the T_i being as weakly correlated as possible. Hence, we should first address the question of how large these correlations are. For the reader's convenience, we recall that our T_i are defined in eqs. (2.6), (2.10), (2.17) and (2.19) and that we also introduced a *complex-MAOS-solution* criterion at the end of section 2.3.3. Two-dimensional plots of the $\Delta T_i(P_W, P_R) - \Delta T_j(P_W, P_R)$ correlations are shown in figure 6. These plots do not include events with complex solutions.

The following comments are in order. First, it is apparent that T_1 and T_2 have a quite strong correlation. This is because the $m_{b\ell}$ value is directly used in the calculation of M_{T2}, that is a monotonically increasing function of $m_{b\ell}$. Further, the MAOS-related variables, T_3 and T_4, are expected to have some degree of correlation with respectively T_1 (related to $m_{b\ell}$) or T_2 (related to $M_{T2}^{t\bar{t}}$). Arguments in support of this statement go as follows. Concerning the $T_3 - T_1$ correlation, $m_t^{\rm maos}$ was defined as

$$(m_t^{\rm maos})^2 = m_{b\ell}^2 + 2\left(\sqrt{(m_{b\ell})^2 + |\mathbf{p}_{b\ell}|^2}|\mathbf{k}^{\text{maos-}WW}| - \mathbf{p}_{b\ell}\cdot\mathbf{k}^{\text{maos-}WW}\right),$$

whence the dependence on $m_{b\ell}$ is apparent. With regards to the $T_4 - T_2$ correlation, recall instead that the $m_{b\ell}$ value was used when calculating $k^{\text{maos-t}\bar{\text{t}}}$, in turn necessary for $m_W^{\rm maos}$. However, in practice, these correlations turn out to be rather weak, and this occurs because of the nontrivial structure of the MAOS solutions. For example, if $M_{T2}^{t\bar{t}}$ is calculated from a balanced configuration, $m_t^{\rm maos}$ can also be written as

$$\begin{aligned}(m_t^{\rm maos})^2 &= m_{b\ell}^2 + 2\left(\sqrt{(m_{b\ell})^2 + |\mathbf{p}_{T,b\ell}|^2}|\mathbf{k}_T|\cosh(\eta_{b\ell}-\eta_\nu) - \mathbf{p}_{T,b\ell}\cdot\mathbf{k}_T\right)\\ &= \left(M_{T2}^{t\bar{t}}\right)^2 + 2\sqrt{(m_{b\ell})^2 + |\mathbf{p}_{T,b\ell}|^2}|\mathbf{k}_T|\left[\cosh(\eta_{b\ell}-\eta_\nu) - 1\right], \qquad (3.1)\end{aligned}$$

for given $\mathbf{k}_T$ values. Therefore, we can regard each of $\{T_3, T_4\}$ vs. each of $\{T_1, T_2\}$ as approximately uncorrelated.

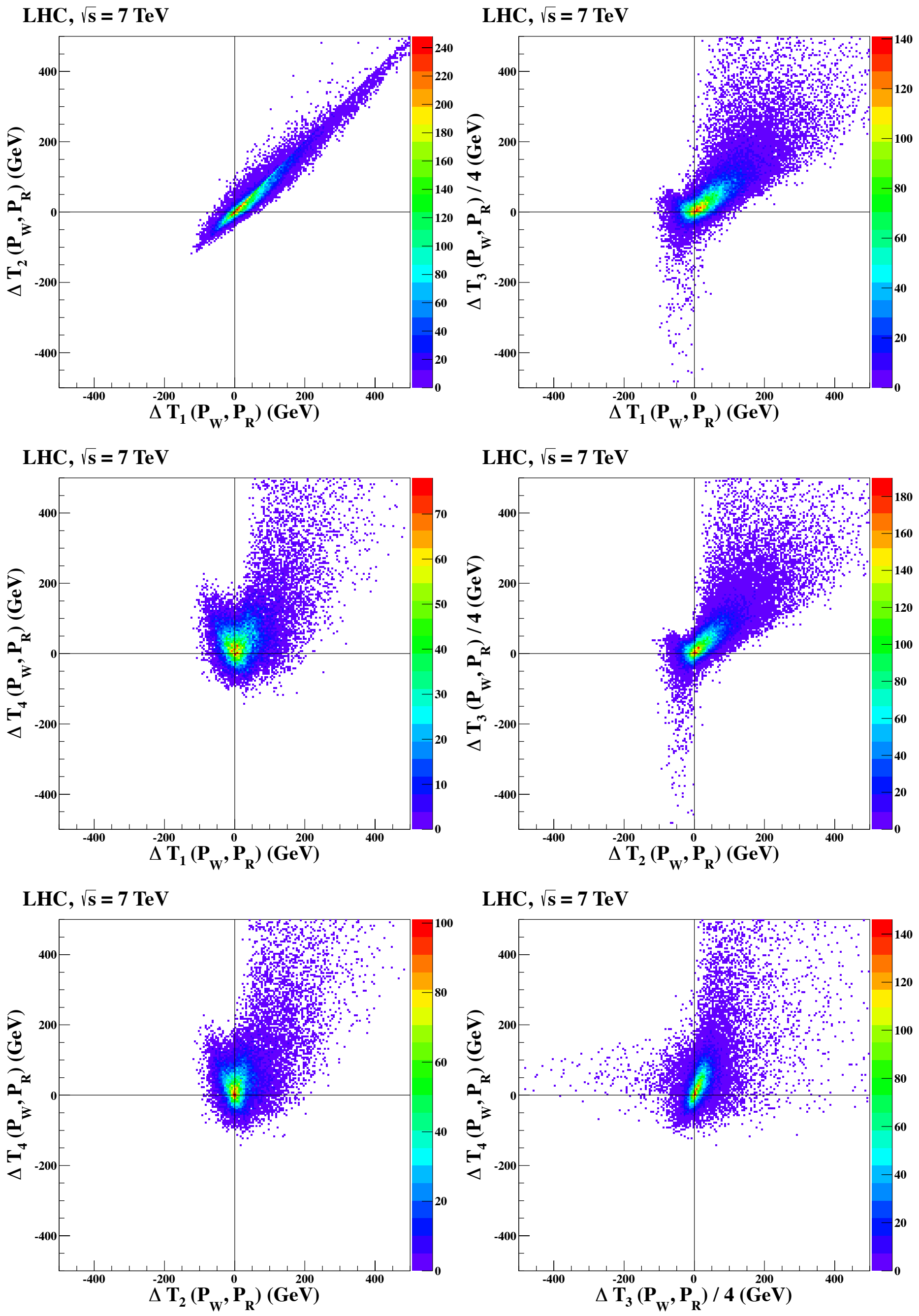

Figure 6. Plots of the correlations between $\Delta T_i(P_W, P_R)$ and $\Delta T_j(P_W, P_R)$. The color code refers to the number of events in each plot pixel.

In principle, one can merge the information from the various T_i even in presence of correlations among them, e.g. by constructing a likelihood function (not to mention more sophisticated pattern-finding techniques such as neural networks). The exploration of optimal ways of using the combined information from all the T_i is of course beyond the scope of the present paper. Besides, it should be emphasized that each of the introduced variables can actually be defined in a number of variations. One may adopt the approach of considering all these variations and using their information in a joint way, that properly takes into account correlations. This approach would also offer a way to improve the method efficiency. We refrain from entertaining such approach in this paper, which is devoted to the discussion of the main ideas behind each variable.

Here we limit ourselves to show that even a very simple combination of the test variables results in an appreciable improvement of the overall method efficiency. We choose $\{T_2, T_3, T_4\}$ as a set of independent test variables. Then, the arguably simplest algorithm to find the right partition by using these variables in a combined test is as follows:

0. Calculate T_2, T_3 and T_4 for the two possible partitions: P_1 and P_2;

1. If $T_1(P_i) > m_{b\ell}^{\max}$ or $T_2(P_i) > m_t$, regard P_i as the wrong partition;

2. If $T_4(P_i)$ results in complex MAOS solutions, whereas no complex solutions are present for the other partition, regard P_i as the wrong partition;

3. If none of the above criteria is met, then choose $P_1(P_2)$ as the right partition if the majority of $\Delta T_i(P_2, P_1) > 0$ (< 0).[8]

Point 1 corresponds to the already mentioned, and well-known, observation that $m_{b\ell}$ and $M_{T2}^{t\bar{t}}$ have a physical upper bound at $m_{bl}^{\max}$ and m_t respectively, if the partition is the correct one. Point 2 is the complex-MAOS-solution criterion enunciated at the end of section 2.3.3. As also discussed there, this method selects the right partition for 98.4% of the events with at least one complex solution. According to our simulation, the combined algorithm 0-3 described above returns the right partition for 89% of the full data set, which we find an already remarkable improvement over the single-variable efficiency.

3.2 Improving by cuts on kinematic variables

Up to this point, we have not introduced any event selection cuts, except for the basic cuts described in section 2.2, that, we checked, have only a marginal impact on the T_i efficiencies. Although the previous section shows that a method efficiency of 90% or even larger is arguably obtainable by just a wise combination of the T_i, we would like to show in this section that improvements are possible also by imposing appropriate kinematic variable cuts. This of course comes at the price of losing (some) event statistics.

First, we note that the property of the test variables of being larger when evaluated with the wrong partition becomes more marked as the final states are more energetic. Intuitively, the larger the magnitude of the input kinematics, the more spread becomes the distribution of the variable, if it is calculated with the wrong partition. On the other hand, the distribution calculated with the right partition enjoys the same physical endpoints independently, of course, of the input kinematics. So, for a more boosted subset of events, one expects $\Delta T_i(P_W, P_R)$ to be larger than zero more often. To single out such event subset,

[8] A more refined approach along the lines of point 3 is to construct a function of the T_i, e.g., $\prod_i T_i$ or a linear combination of T_i's, and choose one partition using the criterion $f(T_i)(P_W) > f(T_i)(P_R)$. We found this kind of approach to also improve efficiency. The likelihood function is just one of such functions.

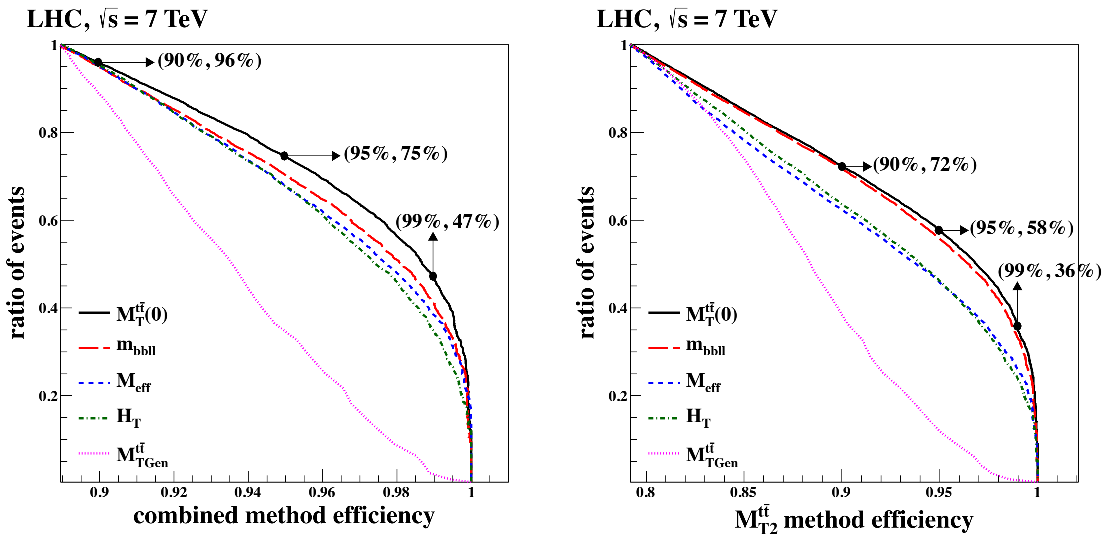

Figure 7. (Left panel) Combined method efficiency vs. loss in statistics with the inclusion of an inclusive cut. The x-axis represents the efficiency of the combined method described in section 3.1 whereas the y-axis reports the number of events that passed one of the inclusive cuts, listed with different line/color codes in the legend. Events are normalized to the event subset that passed the basic selection cuts discussed in section 2.2. (Right panel) Same as the left panel, but for the T_2 variable only, rather than the combined method, on the x-axis.

one may enforce cuts on appropriate kinematic variables, and parametrically improve the method efficiency as the cut gets stronger.

For the dileptonic $t\bar{t}$ process, a well-known set of 'partition-insensitive' kinematic variables — which namely treat all the visible particles on an equal footing, hence they are free of combinatorial ambiguities — is represented by:

- $M_T^{t\bar{t}}(0)$,
- $m_V^2 \equiv (p_{b_1} + p_{b_2} + p_{\ell_1} + p_{\ell_2})^2$,
- $M_{\rm eff} = \sum_i p_{iT} + |\not{\mathbf{p}}_T|$,
- $H_T = \sum_i p_{iT}$, where $i = b_1,\, b_2,\, \ell_1,\, \ell_2$,
- $M_{T{\rm Gen}}^{t\bar{t}}$,

where $M_T^{t\bar{t}}(0)$ is the transverse mass of the full $t\bar{t}$ system with $m_{\nu\nu} = 0$ [34, 41, 42],

$$\left(M_T^{t\bar{t}}(0)\right)^2 \equiv m_V^2 + 2\left(\sqrt{|\mathbf{p}_T|^2 + m_V^2}\,|\not{\mathbf{p}}_T| - \mathbf{p}_T \cdot \not{\mathbf{p}}_T\right) \quad \text{with } \mathbf{p} \equiv \sum_{i=b,\,\ell} \mathbf{p}_i\,, \tag{3.2}$$

and $M_{T{\rm Gen}}^{t\bar{t}}$ is the smallest value of $M_{T2}^{t\bar{t}}$ obtained over all possible partitions [25]. One can impose these cuts in addition to the basic event selection cuts of section 2.2. In the left panel of figure 7, we show the flow of method efficiency vs. loss in statistics as one makes the cuts harder. See figure caption for full details.

The figure shows that the most effective cut variable is $M_T^{t\bar{t}}(0)$. One can reach 90% method efficiency (i.e. get the right partition 90% of the times) with just a 4% loss in event statistics. The efficiency rises to 99% when roughly halving the statistics. For the sake of completeness, we also mention that, for the quoted efficiencies of 90%, 95% and 99%, the cut value is respectively $M_T^{t\bar{t}}(0) > 277$, 343 and 404 GeV.

Because, for some event topologies to be described in the next section, the MAOS-based variables T_3 and T_4 are not usable, but the M_{T2}-based variable T_2 still is, we also show in the right panel of figure 7 a plot of efficiency gain vs. statistics loss for the T_2 variable alone.

4 Generalizations of the method

4.1 Case of chain-assignment as well as ordering ambiguities

From the discussion so far, our method of finding the right partition can be promptly generalized, in particular to topologies relevant for new physics scenarios. Among the most popular such event topologies is the one in eq. (2.7), that is, pair-production of heavy particles, decaying into a set of visible particles plus a pair of invisible particles (possibly, dark-matter candidates). We here sketch this generalization, leaving full details to future work [14]. For the sake of discussion, we here focus on identical decay chains, but the argument presented below can be extended also to the case of non-identical decay chains.

The first observation to make is that the decay of heavy parent particles can be in one step or multiple steps, depending on the mass spectrum and couplings of the new particles. The T_1 and T_2 variables of sections 2.3.1 and 2.3.2 can be defined, and applied to find the right partition of the visible particles, even in the case of a one-step decay, e.g., gluino-pair production, followed by the three-body decay $\tilde{g} \to qq\tilde{\chi}_1^0$ in R-parity conserving supersymmetric models. On the other hand, to utilize the MAOS-based variables T_3 and T_4, the decay process should be at least in two steps, as e.g. the dileptonic $t\bar{t}$ process is. For instance, if $m_{\tilde{q}} < m_{\tilde{g}}$, gluino-pair production will be dominantly followed by two-step decays, i.e., $\tilde{g} \to q\tilde{q} \to qq\tilde{\chi}_1^0$. In terms of event topology, the cascade decay processes of interest to this discussion can be generalized as

$$\begin{aligned} Y\bar{Y} &\to V_1(p_1)X_1 + V_1'(p_1')X_1' \to V_1(p_1)V_2(p_2)X_2 + V_1'(p_1')V_2'(p_2')X_2' \\ &\to \cdots \to V_1(p_1)\cdots V_n(p_n)\chi(k_1) + V_1'(p_1')\cdots V_n'(p_n')\bar{\chi}\ (k_2)\,, \end{aligned} \tag{4.1}$$

for $m_Y > m_{X_1} > m_{X_2} > \cdots > m_\chi$ and $m_{\bar{Y}} > m_{X_1'} > m_{X_2'} > \cdots > m_{\bar{\chi}}$. This decay is also sketched in figure 4.1. The rest of the present discussion will also assume $m_{X_i} = m_{X_i'}$, albeit this requirement is renounceable with appropriate modifications of the method.

The second observation is that, in the context of this general event topology, there is, when partitioning the visible particles, an *additional* type of combinatorial ambiguity with respect to dileptonic $t\bar{t}$. It is the *ordering* ambiguity, corresponding to the fact that $V_a^{(\prime)}$ is produced before $V_{a+1}^{(\prime)}$ $(a = 1, \cdots, n-1)$. Of course, there is still, as in dileptonic $t\bar{t}$, the

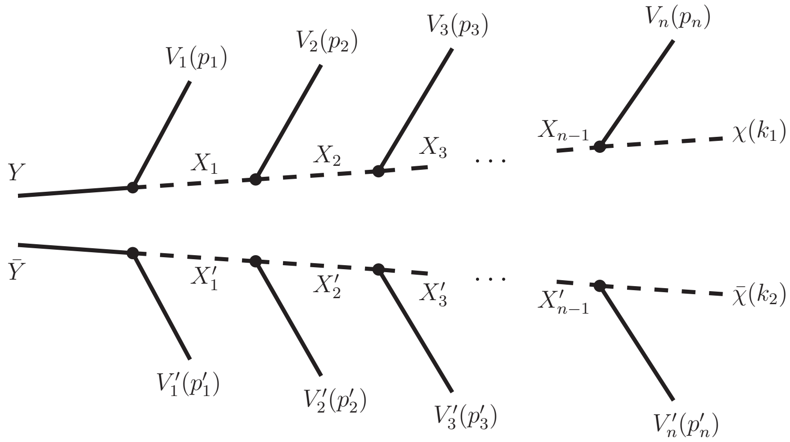

Figure 8. The decay process of eq. (4.1). The momenta p_i and p'_i are assumed to be measurable, while k_i give rise to missing transverse momentum.

combinatorial ambiguity of *pairing* the visible particles into two sets, i.e., distinguishing $\{V_a\}$ from $\{V'_a\}$. Then, the total number of partitions of the visible particles is

$$N = (\text{number of pairings}) \times (\text{number of orderings in one chain})^2 = \frac{{}_{2n}C_n}{2} \times (n!)^2 \,, \quad (4.2)$$

if the visible particles are not distinguishable among each other, as is the case for jets (barring taggings etc.). Then, one can calculate the MAOS invariant masses of $2n$ parent particles (Y, $X_1, \cdots, X_{n-1}$, $\bar{Y}$, $X'_1, \cdots, X'_{n-1}$), such that n MAOS-based test variables are defined. We will label them as T_a^{maos} ($a = 0, \cdots, n-1$), for a given partition P_j ($j = 1, \cdots, N$) and MAOS momenta k^{maos} (we recall that the MAOS determination of the invisible momenta consists in general of several solutions, collectively indicated as k^{maos}). Thence, one can define:

$$T_a^{\text{maos}}(P_j,\, k^{\text{maos}}) \equiv \sum_{c=1,2;\,\alpha=+,-} |\Delta_{X_a} m_{X_a}^{\text{maos}}(p_{a\,c},\, k_c^\alpha)|(P_j)\,, \quad (4.3)$$

where

$$\Delta_{X_a} m_{X_a}^{\text{maos}}(p_{a\,c}, k_c^\alpha) \equiv m_{X_a}^{\text{maos}}(p_{a\,c},\, k_c^\alpha) - m_{X_a} \quad (4.4)$$

with $p_{a\,1} \equiv \sum_{j=a+1}^n p_j$, $p_{a\,2} \equiv \sum_{j=a+1}^n p'_j$, and $X_0 = Y$. These correspond to the T_3 and T_4 variables discussed in section 2.3.3. Actually, each $T_a^{\text{maos}}(P_j,\, k^{\text{maos}})$ can be obtained in different ways, since the MAOS momenta k^{maos} can be calculated from ${}_nC_2$ subsystems. In order to account for them in a symmetric way, one may define T_a^{maos} as

$$T_a^{\text{maos}}(P_j) \equiv \sum_{\forall k^{\text{maos}}} T_a^{\text{maos}}(P_j,\, k^{\text{maos}})\ . \quad (4.5)$$

Each $T_a^{\rm maos}$ variable can then be used to decide on the right partition: this partition is likely to have the smallest $T_a^{\rm maos}$ value than all the other partitions, irrespective of whether combinatorial ambiguities concern the pairing or the ordering of the visible particle sets.

The T_1 and T_2 variables are also usable because one can calculate several subsystem T_1's and T_2's. For example, in the event topology (4.1), the subsystem T_2, or briefly $T_2^{\rm sub}$, can be defined as $T_2^{Y\bar{Y}}$, $T_2^{X_1X_1'}$, $\cdots$, $T_2^{X_{n-1}X_{n-1}'}$, such that $T_2^{Y\bar{Y}} \leq m_Y$, $T_2^{X_1X_1'} \leq m_{X_1}$, $\cdots$, $T_2^{X_{n-1}X_{n-1}'} \leq m_{X_{n-1}}$ for the right partition. By sequentially testing the partitions in the order $Y\bar{Y} \to \cdots \to X_{n-1}X_{n-1}'$ systems, at each step selecting the partition with the smallest $T_2^{\rm sub}$, one can find the most likely partition for the full system.

We finally observe that the information from the above test variables can be merged into a combined method in various ways. The simplest algorithm may be

(i) Calculate all the test variables as explained above. If $T_1^{X_aX_a'} > m^{\rm max}_{V_{a+1}\cdots V_n} = m^{\rm max}_{V_{a+1}'\cdots V_n'}$ or $T_2^{X_aX'_a} > m_{X_a}$ for $a = 0, \cdots, n-2$ or there are more complex MAOS solutions in a given partition P_j than in any other partition, one should regard P_j as the wrong one.

(ii) If the above procedure fails to pick up one partition, one may select the right partition P_j from the requirement that it gives the smallest value of T_i (with respect to the other partitions) for the largest number of test variables.

We again emphasize that the efficiency of each T_i and of the combined method can be further improved by imposing cuts on 'partition-insensitive' variables, as discussed in section 3.2.

Concrete examples of this generalized method will be the gluino pair-production and decay discussed above, and the pair-production of the second lightest neutralino $\tilde{\chi}_2^0$, which decays to $\ell^+\ell^-\tilde{\chi}_1^0$. We will consider in more details these new physics processes for certain benchmark points in future work [14].

4.2 Comments about the method's dependence on mass information

We would like to conclude this section about generalizations with a few remarks about the question of the method's dependence on the knowledge of the mass of the pair-produced states, m_Y, or that of the invisible daughters, m_χ.[9] As a first remark, we emphasize again that, of our proposed T_i, the variables T_1 as well as T_2 do not use the information on m_Y at all. On the other hand, this information appears necessary for constructing the MAOS-based variables T_3 and T_4, at least according to the way they were defined in section 2.3.3. In order to be able to use the variables $T_{3,4}$ at all, one would therefore seem to need m_Y and m_χ to have been measured already.

It is worth observing that, in many scenarios of new physics, the mass measurements in question are not expected to be affected by combinatorial ambiguities. This holds in particular in the case of the topologies of interest for our method, where one can construct the event variable M_{T2}. In fact, if, in absence of combinatorial ambiguities, m_Y may be

[9]We thank the Referee for triggering this discussion.

estimated from the endpoint of M_{T2}, then, in presence of combinatorial ambiguities, the same estimate can be performed using $M_{T\mathrm{Gen}}$ [25] instead, i.e. the smallest M_{T2} value for all possible partitions, which enjoys the same endpoint position as M_{T2} constructed with the right partition.[10] In cases where the production cross-section is so small, or background contamination so high, that the mass information cannot practically be extracted along the above lines, one can consider using a modified version of our MAOS-based variables, wherein the parametric dependence on the true value of m_Y is disposed of. To make an example, in place of the T_3 definition, given in eq. (2.17), one may instead use the quantity

$$\tilde{T}_3(P_k) \;\equiv\; |m_t^{\mathrm{maos}}(\text{chain } 1) - m_t^{\mathrm{maos}}(\text{chain } 2)|\,, \tag{4.6}$$

which should be close to zero if the partition is the correct one, whereas it can be much larger if the partition is wrong. Hence, again, $\Delta\tilde{T}_3(P_W, P_R)$ is expected to prefer positive values. We note explicitly that the notation in eq. (4.6) is, similarly as in eq. (2.14), incomplete, in that the MAOS solution obtained from the on-shell relations (2.11) is not unique (see discussion below those relations). On the other hand, on the r.h.s. of eq. (2.11), one does *not necessarily* have to choose the parent particle mass. One has in general the following choices [34]

- MAOS1: m_Y [9]
- MAOS2: $M_{T2} = \min_{\vec{p}_{\chi_1,T}+\vec{p}_{\chi_2,T}=\not{p}_T} \max\{M_T^{(1)}, M_T^{(2)}\}$
- MAOS3: $M_T^{(i)}$, with $i = 1, 2$ labeling the decay chain.

The advantage of MAOS3 is that it allows to have a *unique* MAOS solution for each event, thereby allowing use of the $\tilde{T}_3$ variable as defined in eq. (4.6). In fact, we found the performance of $\Delta\tilde{T}_3$ comparable to that of ΔT_3, as defined in section 2.3.3. The reason why we defined our MAOS-based variables according to the MAOS1 scheme is mostly simplicity.

The other unknown mass besides m_Y is m_χ, upon which all the T_i variables bear dependence. While the necessity to input some m_χ value seems inescapable, we are actually quite confident that our method would perform rather well even in the case where the m_χ mass is yet to be measured at the moment of having to solve the combinatorial problem. We make the following considerations in support of this statement. First, as already mentioned in the general M_{T2} discussion in section 2.3.2, an estimate, perhaps an accurate one, of m_χ may be obtained from the M_{T2} kink [17–20], which however requires sufficient statistics. Even in absence of such statistics, and in presence of combinatorial ambiguities, the uppermost part of the $M_{T\mathrm{Gen}}(m_\chi)$ plot in the m_χ vs. m_Y plane may provide a rough idea of the m_χ mass. It is worth emphasizing that a rough input value for m_χ may well be sufficient in many scenarios. It is so at least in the case where $m_\chi \ll m_Y$: it can be shown in fact [43] that, in this limit, MAOS solutions have corrections going as m_χ^2/m_Y^2 and are, therefore, largely insensitive to the specific value chosen for m_χ, so long as the mentioned mass hierarchy holds at least approximately.

[10] The use of $M_{T\mathrm{Gen}}$ was also invoked in section 3.2 as a partition-insensitive cut variable.

Clearly, all the issues mentioned in this section deserve further investigation, which is best carried out within specific new-physics benchmark points. This lies outside the scope of the present paper, mainly meant to propose our method and to apply it to the simplest yet relevant SM example we could think of, namely $t\bar{t}$ production. We will however return to all these issues in a forthcoming paper [14].

5 Conclusions and outlook

In this paper, we have proposed a novel method to resolve combinatorial ambiguities in hadron collider events involving two invisible particles in the final state. This method is based on the kinematic variable M_{T2} and on the MAOS reconstruction of invisible momenta, that are reformulated as test variables T_i, namely testing the correct combination against the incorrect ones. The efficiency of each single T_i in the determination of the correct combination can then be systematically improved in two directions: by combining the information from the different T_i and by introducing further cuts on suitable, partition-insensitive, variables. In this sense, our method is completely scalable.

All the above program is illustrated in the specific, and *per se* interesting example of top anti-top production, followed by a leptonic decay of the W on both sides. We however emphasize that, by construction, our method is also directly applicable to many topologies of interest for new physics, in particular events producing a pair of undetected particles, that are potential dark-matter candidates.

Our method opens a whole spectrum of generalizations and by-product issues, on which work is in progress [14]. The most urgent include:

- Addressing whether and how the method is affected by the inclusion of effects such as QCD radiation, hadronization and signal degradation due to detector effects. The main challenge of this problem is that, after hadronization, the assignment of a 'parton' to a given decay chain or to a certain position within the decay chain is no more well-defined. As such, it requires separate thought.

- Generalizing the method to the combinatorial uncertainty due to the *ordering* of the visible particles in the decay chain, uncertainty which is not present in dileptonic $t\bar{t}$.

Acknowledgments

KC and DG gratefully acknowledge the hospitality of Universidad Autónoma de Madrid and CSIC, as well as of CERN (the TH-LPCC Summer Institute on LHC Physics) where part of this work was carried out. We would like to thank W. S. Cho and Y. G. Kim for the discussion that laid the foundation for this work. KC is supported by the KRF Grants funded by the Korean Government (KRF-2008-314-C00064 and KRF-2007-341-C00010) and the KOSEF Grant funded by the Korean Government (No. 2009-0080844). The work of DG is supported by the EU Marie Curie IEF Grant no. PIEF-GA-2009-251871. The work of CBP is partially supported by the grants FPA2010-17747, Consolider-CPAN (CSD2007-00042) from the MICINN, HEPHACOS-S2009/ESP1473 from the C. A. de Madrid and the contract "UNILHC" PITN-GA-2009-237920 of the European Commission.

JHEP11(2011)117

References

[1] A.J. Barr and C.G. Lester, *A review of the mass measurement techniques proposed for the large hadron collider*, *J. Phys. G* **G 37** (2010) 123001 [arXiv:1004.2732] [INSPIRE].

[2] A. Rajaraman and F. Yu, *A new method for resolving combinatorial ambiguities at hadron colliders*, *Phys. Lett.* **B 700** (2011) 126 [arXiv:1009.2751] [INSPIRE].

[3] G. Mahlon and S.J. Parke, *Angular correlations in top quark pair production and decay at hadron colliders*, *Phys. Rev.* **D 53** (1996) 4886 [hep-ph/9512264] [INSPIRE].

[4] T. Stelzer and S. Willenbrock, *Spin correlation in top quark production at hadron colliders*, *Phys. Lett.* **B 374** (1996) 169 [hep-ph/9512292] [INSPIRE].

[5] G. Mahlon and S.J. Parke, *Maximizing spin correlations in top quark pair production at the Tevatron*, *Phys. Lett.* **B 411** (1997) 173 [hep-ph/9706304] [INSPIRE].

[6] G. Mahlon and S.J. Parke, *Spin correlation effects in top quark pair production at the LHC*, *Phys. Rev.* **D 81** (2010) 074024 [arXiv:1001.3422] [INSPIRE].

[7] C. Lester and D. Summers, *Measuring masses of semiinvisibly decaying particles pair produced at hadron colliders*, *Phys. Lett.* **B 463** (1999) 99 [hep-ph/9906349] [INSPIRE].

[8] A. Barr, C. Lester and P. Stephens, *m_{T2} the truth behind the glamour*, *J. Phys. G* **G 29** (2003) 2343 [hep-ph/0304226] [INSPIRE].

[9] W.S. Cho, K. Choi, Y.G. Kim and C.B. Park, *m_{T2}-assisted on-shell reconstruction of missing momenta and its application to spin measurement at the LHC*, *Phys. Rev.* **D 79** (2009) 031701 [arXiv:0810.4853] [INSPIRE].

[10] J. Alwall, M. Herquet, F. Maltoni, O. Mattelaer and T. Stelzer, *MadGraph 5 : going beyond*, *JHEP* **06** (2011) 128 [arXiv:1106.0522] [INSPIRE].

[11] M. Aliev, H. Lacker, U. Langenfeld, S. Moch, P. Uwer, et al., *HATHOR: HAdronic Top and Heavy quarks crOss section calculatoR*, *Comput. Phys. Commun.* **182** (2011) 1034 [arXiv:1007.1327] [INSPIRE].

[12] P.M. Nadolsky, H.-L. Lai, Q.-H. Cao, J. Huston, J. Pumplin, et al., *Implications of CTEQ global analysis for collider observables*, *Phys. Rev.* **D 78** (2008) 013004 [arXiv:0802.0007] [INSPIRE].

[13] ATLAS collaboration, *Measurement of the top quark pair production cross section in pp collisions at $\sqrt{s} = 7\,TeV$ in dilepton final states with ATLAS*, ATLAS-CONF-2011-100 (2011).

[14] K. Choi, D. Guadagnoli, and C. B. Park, in preparation.

[15] J. Smith, W. van Neerven and J. Vermaseren, *The transverse mass and width of the W boson*, *Phys. Rev. Lett.* **50** (1983) 1738 [INSPIRE].

[16] V.D. Barger, A.D. Martin, and R. Phillips, *Perpendicular e neutrino mass from W decay*, *Z. Phys.* **C 21** (1983) 99.

[17] W.S. Cho, K. Choi, Y.G. Kim and C.B. Park, *Gluino stransverse mass*, *Phys. Rev. Lett.* **100** (2008) 171801 [arXiv:0709.0288] [INSPIRE].

[18] W.S. Cho, K. Choi, Y.G. Kim and C.B. Park, *Measuring superparticle masses at hadron collider using the transverse mass kink*, *JHEP* **02** (2008) 035 [arXiv:0711.4526] [INSPIRE].

[19] B. Gripaios, *Transverse observables and mass determination at hadron colliders*, *JHEP* **02** (2008) 053 [arXiv:0709.2740] [INSPIRE].

[20] A.J. Barr, B. Gripaios and C.G. Lester, *Weighing wimps with kinks at colliders: invisible particle mass measurements from endpoints*, *JHEP* **02** (2008) 014 [arXiv:0711.4008] [INSPIRE].

[21] M.M. Nojiri, K. Sakurai, Y. Shimizu and M. Takeuchi, *Handling jets + missing E_T channel using inclusive m_{T2}*, *JHEP* **10** (2008) 100 [arXiv:0808.1094] [INSPIRE].

[22] M. Burns, K. Kong, K.T. Matchev and M. Park, *Using subsystem m_{T2} for complete mass determinations in decay chains with missing energy at hadron colliders*, *JHEP* **03** (2009) 143 [arXiv:0810.5576] [INSPIRE].

[23] K. Choi, D. Guadagnoli, S.H. Im and C.B. Park, *Sparticle masses from transverse-mass kinks at the LHC: the case of Yukawa-unified SUSY GUTs*, *JHEP* **10** (2010) 025 [arXiv:1005.0618] [INSPIRE].

[24] K. Choi, J.S. Lee and C.B. Park, *Measuring the Higgs boson mass with transverse mass variables*, *Phys. Rev.* **D 82** (2010) 113017 [arXiv:1008.2690] [INSPIRE].

[25] C. Lester and A. Barr, *MTGEN: mass scale measurements in pair-production at colliders*, *JHEP* **12** (2007) 102 [arXiv:0708.1028] [INSPIRE].

[26] W.S. Cho, K. Choi, Y.G. Kim and C.B. Park, *Measuring the top quark mass with m_{T2} at the LHC*, *Phys. Rev.* **D 78** (2008) 034019 [arXiv:0804.2185] [INSPIRE].

[27] J. Alwall, K. Hiramatsu, M.M. Nojiri and Y. Shimizu, *Novel reconstruction technique for new physics processes with initial state radiation*, *Phys. Rev. Lett.* **103** (2009) 151802 [arXiv:0905.1201] [INSPIRE].

[28] CDF Collaboration collaboration, T. Aaltonen et al., *Top quark mass measurement using m_{T2} in the dilepton channel at CDF*, *Phys. Rev.* **D 81** (2010) 031102 [arXiv:0911.2956] [INSPIRE].

[29] P. Konar, K. Kong, K.T. Matchev and M. Park, *Dark matter particle spectroscopy at the LHC: generalizing m_{T2} to asymmetric event topologies*, *JHEP* **04** (2010) 086 [arXiv:0911.4126] [INSPIRE].

[30] E.L. Berger, Q.-H. Cao, C.-R. Chen, G. Shaughnessy and H. Zhang, *Color sextet scalars in early LHC experiments*, *Phys. Rev. Lett.* **105** (2010) 181802 [arXiv:1005.2622] [INSPIRE].

[31] M.M. Nojiri and K. Sakurai, *Controlling ISR in sparticle mass reconstruction*, *Phys. Rev.* **D 82** (2010) 115026 [arXiv:1008.1813] [INSPIRE].

[32] H. Zhang, E.L. Berger, Q.-H. Cao, C.-R. Chen and G. Shaughnessy, *Color sextet vector bosons and same-sign top quark pairs at the LHC*, *Phys. Lett.* **B 696** (2011) 68 [arXiv:1009.5379] [INSPIRE].

[33] E.L. Berger, Q.-H. Cao, C.-R. Chen, C.S. Li and H. Zhang, *Top quark forward-backward asymmetry and same-sign top quark pairs*, *Phys. Rev. Lett.* **106** (2011) 201801 [arXiv:1101.5625] [INSPIRE].

JHEP11(2011)117

[34] C.B. Park, *Reconstructing the heavy resonance at hadron colliders*, *Phys. Rev.* **D 84** (2011) 096001 [arXiv:1106.6087] [INSPIRE].

[35] H. Murayama, M. Nojiri and K. Tobioka, *Improved discovery of a nearly degenerate model: MUED using m_{T2} at the LHC*, arXiv:1107.3369 [INSPIRE].

[36] D0 Collaboration collaboration, B. Abbott et al., *Measurement of the top quark mass using dilepton events*, *Phys. Rev. Lett.* **80** (1998) 2063 [hep-ex/9706014] [INSPIRE].

[37] D0 Collaboration collaboration, V.M. Abazov et al., *Measurement of the top quark mass in final states with two leptons*, *Phys. Rev.* **D 80** (2009) 092006 [arXiv:0904.3195] [INSPIRE].

[38] D0 Collaboration collaboration, V.M. Abazov et al., *Measurement of spin correlation in $t\bar{t}$ production using dilepton final states*, *Phys. Lett.* **B 702** (2011) 16 [arXiv:1103.1871] [INSPIRE].

[39] C. Lester, *The Oxbridge m_{T2} / stransverse mass library*, http://www.hep.phy.cam.ac.uk/~lester/mt2/index.html.

[40] B. Gripaios, K. Sakurai and B. Webber, *Polynomials, Riemann surfaces and reconstructing missing-energy events*, *JHEP* **09** (2011) 140 [arXiv:1103.3438] [INSPIRE].

[41] A.J. Barr, B. Gripaios and C.G. Lester, *Measuring the Higgs boson mass in dileptonic W-boson decays at hadron colliders*, *JHEP* **07** (2009) 072 [arXiv:0902.4864] [INSPIRE].

[42] D.R. Tovey, *Transverse mass and invariant mass observables for measuring the mass of a semi-invisibly decaying heavy particle*, *JHEP* **11** (2010) 148 [arXiv:1008.3837] [INSPIRE].

[43] W.S. Cho, K. Choi and C.B. Park, unpublished.

JHEP11(2011)117